Influence of Coaxial Nozzle Design on Atomization of Cell Suspensions and Cell Survival Rate

Georg Möller[1*], Sarah Klein[2], Anja Lena Thiebes[2], Christian G. Cornelissen[2], Manuel A. Reddemann[1]
[1]Institute of Heat and Mass Transfer, RWTH Aachen University, Germany
[2]Department of Biohybrid & Medical Textiles (BioTex), AME - Institute of Applied Medical Engineering, Helmholtz Institute, RWTH Aachen University, Germany
*Corresponding author: moeller@wsa.rwth-aachen.de

Abstract
Using stem cells as method of treatment for Acute Respiratory Distress Syndrome or Chronic Obstructive Pulmonary Disease is a technique of rising interest. High concentrations of stem cells in the area of interest are vital to enhance the effect of this therapy. The authors of this work aim to achieve those concentrations by spraying a high concentrated solution of stem cells into the human airway using bronchoscopes equipped with nozzles specifically designed for this purpose.
The general suitability of coaxial atomization principle has already been proven in earlier studies for one particular nozzle. This work evaluates the potential of nozzle geometry adaptation for improvement of atomization and cell survival rates. Based on the existing coaxial nozzle design, the diameter of the inner annular exit for the liquid phase is varied as well as the thickness of the wall between liquid and gas phase. That way, different exit velocities of the liquid phase as well as different gap sizes between the gas and the liquid phase are achieved leading to noticeable changes in the velocity field of the injected substances while keeping the momentum of the gas phase constant. The influence of nozzle geometry on droplet formation and subsequent cell survival rates is analyzed based on a combination of two different measurement techniques. Sprays are analyzed using a high-speed transmitted microscopy system including adapted post processing, while cell survival rates are evaluated by fluorescence microscopy before and after the atomization process.
Throughout this study, droplet sizes as well as the diameter of the liquid cone at the nozzle exit are found not to be influenced by the variation of the nozzle. In contrast, cell survival rates are increasing with increasing values of the gap between the two phases being proportional to surface instabilities described by the transverse instability wavelength. The disintegration length is also influenced by the variation of the nozzle showing a dependency on the momentum flux ratio of both phases.

Keywords
Coaxial Atomization, CellSpray, Droplet sizes, Patternator, Survival Rates

Introduction

In recent years, stem cell therapy became a growing field of research in regenerative medicine since stem cells support healing processes of various kinds of diseases. The ability of stem cells curing leukaemia results in a well-known and one of the most established cell therapies. In the process of this therapy, stem cells are injected intravenously and thus spreading across the entire body. Furthermore, stem cell therapy can also be applied for treatment of burn injuries [1, 2], topographically difficult or chronic wounds [3] as well as diseases of internal organs [4]. However, in all different treatments high concentrations of stem cells are to be achieved in order to maximize the treatments succes. Thus, the way of applying stem cells in human airways in order to cure the diseases mentioned above is vital for a well designed treatment.
Spraying of stem cells is a promising approach to match the requirement of intrapulmonary stem cell therapy and has the potential of combining high local cell concentrations and sufficient amounts of viable cells. Its suitability for human airways was shown in earlier studies. Thiebes et. al [5] sprayed muscle and epithelial cells using a 2-phase nozzle. The authors noticed a decreasing surivial rate for increasing gas pressures. Furthermore, long term experiments showed, that cells applied via spray are capable of building tissue engineered constructs, if they are exposed to a cell growth medium. Gerlach et. al [6] used cell spray applications for stem cell transplantation in order to treat burn injuries finding that the ratio between treated area and donoring area could noticeably be enlarged by using spray in comparison to traditional transplantation techniques. Similar results were also stated by [7].
However, in order to conduct treatments using stem cells in human airways, stem cells are required to get as far as possible into the complex and narrow geometry of human lungs. Thus, droplet sizes in the same order of magnitude as the cell diameter are favoured as well as small spray angles. Thiebes et. al [8] applied cells by a catheter inserted into a clinical used bronchoscope. The tip of the catheter is equipped with a coaxial nozzle supplying both cell containing liquid and gas phase. The latter ensures atomization of the fluid. Since atomization is caused by several external forces, the process and its boundary conditions have an impact on cell survival rates [9]. Three potential effects such as pressure, spinning and shearing have been found to possibly be responsible for destroying cells in atomization processes [10]. All three of these effects are supposedly relevant, since the atomization process exposes the cells to a combination of high shearing rates and extensional flows, while the cell suspension exits the

nozzle and interacts with the surrounding air flow. Hereby, transversal instabilities cause the formation of ligaments and eventually droplets leading to a noticeably decreasing survival rate of the cells.
In this study, different coaxial nozzles have been used for cell spray experiments. The cell survival rate has been measured across the radius of the spray as well as the global cell survival for different conditions. Furthermore, the influence of different cell concentrations has also been measured.

Material and Methods
This study ist based on a two-step approach. In a first step, the atomization characteristics of cell solutions is investigated by means of in-situ optical diagnostics. In a second step, cell survival rates are quantified by probe measurements. The investigated substances, the test-setup and the experimental methods are described in detail below.

Substances
Experiments are performed using living melanoma cells of human cell line SK-MEL-28 suspended in a phosphate buffered saline (PBS) solution. Before atomization experiments are conducted, the cells are washed and re-suspended in PBS at the designated cell concentration. The cells have a mean diameter of 19.4 µm with a standard deviation of 2.72 µm [11, 12, 13] and thus are suitable as a comparison with stem cells with comparable diameters [14].Since the cells diameter is noticeably larger compared to earlier studies [9], the influence of cell concentrations is investigated in this study. Therefore, experiments with concentrations of 0.2×10^6 cells /mL, 1×10^6 cells /mL and 4×10^6 cells /mL are additionally carried out in order to investigate, if the fluids rheology is noticeably influenced by the cell concentration. The substances are injected at T = 293.15 K and p = 100 kPa so temperatures and pressures match ambient conditions leading to material properties of $\rho_{liq} = 1000\,kg\,m^{-3}$ and $\nu_{liq} = 1.06\,m^2\,s^{-1}$ [15].
To determine survival rate subsequent to cell spraying, cells are first incubated for 20 min in a cell permeable dye for determining cell viability. 4 µM Calcein-AM in PBS (both Thermo Fisher Scientific) was used at 310.15 K and 5% CO2 with a final cell concentration of 1×10^6 cells /mL.

Test Setup
Figure 1 gives an overview of the test setup. The cell suspension is atomized by a coaxial two-fluid nozzle. The resulting spray is collected by a Petri dish respectively by a patternator at an axial distance of 100 mm (cf. figure 1 and 3). The pipe of the atomizer can be changed, leading to values for the inner diameter of d_i =1.2 mm, 1.5 mm and 1.6 mm.

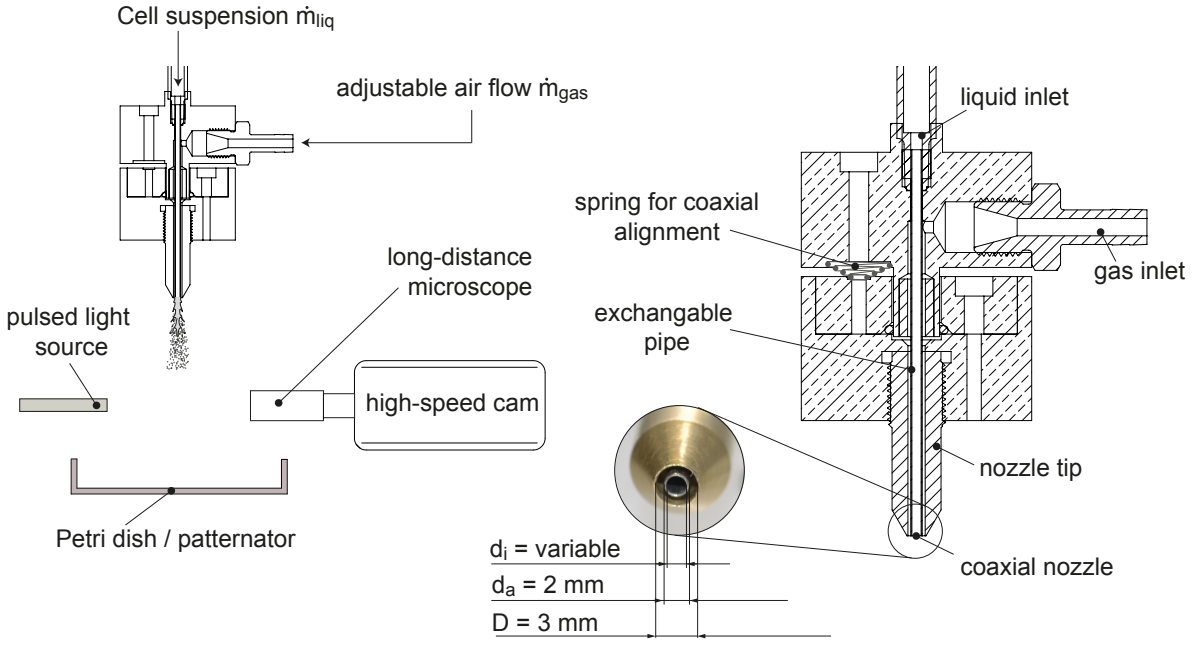

Figure 1. On the left the general test setup used in this study of coaxial atomization is given. For investigations of the radial survival rates, a patternator is applied in contrast to a traditional Petri dish for global survival rates. On the right, a detailed view of the coaxial nozzle including the exchangable pipe is presented.

In contrast, the outer diameter of the pipe d_a is kept constant at 2 mm for every measurement taken (cf. figure 1) leading to a variation in wall thickness of s = 400 µm, 250 µm and 200 µm (cf. figure 2). The pipe is surrounded by an annular flow of air, which is responsible for the atomization of the injected cell suspensions. The outer diameter of the annular gas flow D is also kept constant at 3 mm representing the diameter of the working channel of bronchoscopes [8]. An overview of the different diameters is also given in table 2. As seen in figure 1, the atomizer consists of two

different body parts. The pipe is exclusively mounted to the upper body, which is held in place by three screws connected with three springs mounted in the gap between the two body parts. This construction allows the uppper body and thus the pipe to be tilted relatively to the lower body allowing to adjust the alignment of the pipe relative to the nozzle tip. Hence, concentricity between the exit nozzle and the pipe is ensured for every taken measuring point. Since the cell suspension is directed vertically into the atomizer, the gas inlet is mounted perpendicularly

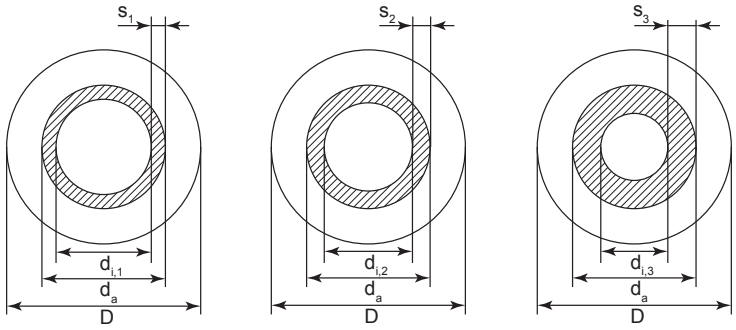

Figure 2. Dimensions of the exchangable pipes.

onto the upper body part. The gas is then forced into a flow straigthener followed by the nozzle exit forming an annular gas flow around the injected cell suspension. The mass flow of cell suspension is kept constant during all experiments while the gas stream is varied between 1.2 $m^3\,h^{-1}$ and 2.1 $m^3\,h^{-1}$ (cf. table 1).

Patternator

A patternator is used enabling the investigation of cell survival rates across the radius of the spray cone. The patternator consists of eleven coaxial chambers as seen in figure 3. The height of the patternators walls has been selected to be 5 mm ensuring droplets not to jump into the adjacent chamber. Since the patternator is built via 3-D-printing production process, the wall thickness is chosen to 0.6 mm. In order to enable transmitted-light microscopy, the patternator is made of a transparent synthetic material.

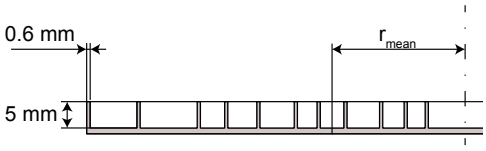

Figure 3. Schematic view on the patternator used for measurements of the radial cell survival rate.

Spray Visualization

A high-speed imaging system consisting of a Fastcam SA-X, Photron Limitied, 1024x1024 is used at 25,000 fps resulting in a 496x1024 image. Microscopic imaging is performed in order to capture primary breakup and droplet propagation. To do so, a long-distance transmitted light microscopy system is applied in combination with a monochromatic and incoherent pulsed light source (Cavilux Smart, 640 nm wavelength, 10 ns pulse duration). A Navitar Mag Zoom Lens with 12:1 zoom ratio set to 9.06 µm/Pixel, resulting in a 4.49 mm x 9.28 mm frame size is installed for this study. Investigations of droplet sizes is undertaken in an adequate distance from the nozzle exit ensuring the influence of primary breakup phenomena to be neglectable. Therefore, the investigated area is inbetween 6 mm and 15.3 mm. This way, the area of fully atomized spray is detected to start 10.65 mm beneath the nozzle exit leading to a frame size of 496x512 pixels. Since the captured frame size is not sufficient to investigate the entire width of the spray, several high-speed videos were taken, scanning the spray horizontally whilst ensuring steady-state atomization conditions. These videos are recombined in image post processing.

Image Post Processing

The image post processing is used to investigate both the disintegration length and droplet sizes of the investigated sprays. For analyzing droplet sizes, each high-speed video is divided into individual images by setting a constant interframing time of 0.4 ms. In contrast to analyzing the video frame by frame, interframing ensures, that slow droplets are not taken into account multiple times because of multiple detection in succesive frames. Every considered frame is then converted into a binary image, which is well suited for detection and evaluation of coherent areas, representing droplets. The amount and location of pixels in coherent areas are recorded and converted into equivalent circle diameters as well as eccentricities. Overlapping droplets can be recorded since a two-dimensional image of a three-dimensional spray is taken, having a high potential for errors in the image processing. These droplets are treated as single droplets with a noticeably higher eccentricity compared to single droplets. In general, droplets with high eccen-

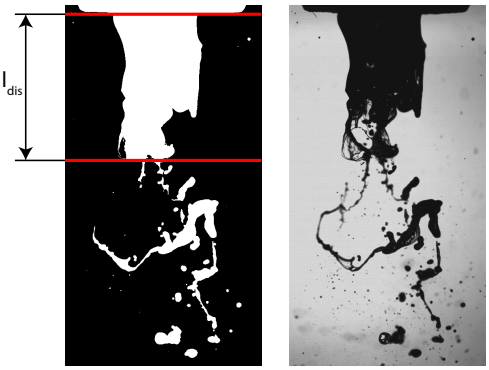

Figure 4. On the left, a binarized image of the spray is given also showing the boundaries in which the disintegration length l_{dis} is evaluated. On the right, the original image is given.

tricities are also known for other error sources such as secondary droplet breakup. Thus, for calculation of Sauter mean diameter (SMD), droplets with eccentricities e > 0.7 are not taken into account resulting in a maximum error potential caused by eccentricity of 5.77%. Droplets, which are off focus, are filtered by two distinct filters with different gamma values, contrasts and grey thresholds. As seen in figure 4, the sensitivity of each filter for intensity gradients is varied enabling the filters to distinguish droplets, that are out of focus. For more information see [15, 9].
Disintegration lengths l_{dis} are derived by visualizing the primary breakup for each investigated test parameter. For this purpose, pixels of coherent areas are counted in each horizontal line of each frame. In order to distinguish between the nozzle and the spray cone (upper red line in figure 4), the number of counted pixels has to undercut the width of the nozzle exit. For determining the disintegration length (lower red line in figure 4) the number of pixels has to fall beneath a minimal threshold, which is selected to represent a fifth of the width at the nozzle exit. In order to minimize the influence of fluctuations in the width of the jet, the threshold value has to be undershot over 100 horizontal lines respectively a length of 0.906 mm.

Test Parameter

Table 1. Investigated parameter set for the gas flow with resulting mass gas-liquid-ratio (GLR), vorticity thickness δ and Weber number constructed on vorticity thickness

Point no.	$\dot{V}_{air}$	$\dot{m}_{air}$	Re_{air}	GLR	δ	We_δ
–	m^3/h	$10^{-3} \cdot kg/s$	–	–	$10^{-5} \cdot m$	–
1	1.2	0.396	5529.8	0.99	3.77	4.41
2	1.5	0.495	6912.3	1.24	3.37	6.17
3	1.8	0.594	8294.7	1.49	3.07	8.12
4	2.1	0.693	9677.2	1.73	2.85	10.23

The air Reynolds number characterizes the gas flow channel as an annular tube between the nozzle tip and the pipe leading to

$$Re_{air} = \frac{u_{air} \cdot 2 \cdot \Delta d}{\nu_{air}} \tag{1}$$

with the gap between these two parts being represented by $\Delta d = (D - d_a)/2$ (cf. figure 2). Since the inner diameter of the pipe is varied throughout this study whilst the liquid mass flow is kept constant, different Reynolds numbers occur for the liquid phase according to equation 2.

$$Re_{liq} = \frac{4 \cdot \dot{m}_{liq}}{d_i \cdot \pi \cdot \eta_{liq}}. \tag{2}$$

The different values for Re_{liq} can be found in table 2.

Table 2. Mass flow and resulting Reynolds numbers of the liquid phase for each of the three pipes

Pipe no.	Inner diameter d_i	Wall thickness	$\dot{m}_{liq}$	Re_{liq}
–	mm	µm	$10^{-3} \cdot kg/s$	$[-]$
1	1.6	200	0.4	300
2	1.5	250	0.4	320
3	1.2	400	0.4	400

Measurement of Survival Rates

As mentioned before, cell survival rates are determined after spraying by recollecting the cell suspension from the Petri dish respectively each chamber of the patternator. The suspension is then analyzed by fluorescence microscopy (AxioObserver Z1, Carl Zeiss) and images are acquired using a high-resolution CCD camera (AxioCam MRm, Carl Zeiss) and AxioVision software. Fluorescence of the cell suspension is achieved by incubation with 4 µM Calcein AM before spraying and propidium iodide (Merck) with a final concentration of 2 µg mL^{-1} after the atomization. The fluorescent radiation with maxima at 495 nm (Calcein) and 617 nm (propidium iodide) is captured and the amount of intact and destroyed cells were recorded (cf. figure 5). Note, that cell survival rates are determined relative to the cell survival rate of an unsprayed control.

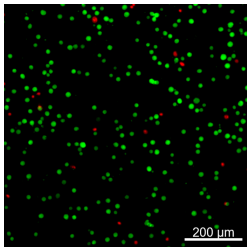

Figure 5. Example of an image taken from the cell suspensions. Intact cells emit radiation in the green spectrum whilst destroyed cells appear to be red.

Results and Discussion

Investigation of spray characteristics such as disintegration length and droplet sizes is conducted for different gas-to-liquid ratios in a two phase coaxial atomizer using a phosphate buffered saline solution enriched with living human cells at various concentrations.

Droplet Sizes

Figure 6 gives the obtained Sauter mean diameters (SMD) showing the influence of cell concentration on mean droplet sizes on the left side. The diameter is slightly decreasing towards higher cell concentrations but, considering the resolution of 9.06 µm/Pixel, the influence is of minor emphasis. This is in good accordance to [9] and [17], where no noticeable differences between a cell suspension and a diluted tris-buffered saline solution without cells were found. In order to ensure this phenomenon, even higher concentrated cell solutions were tested within this study. In fact, in the present ranges of cell suspensions and external forces caused by atomization, the fluids show a strict

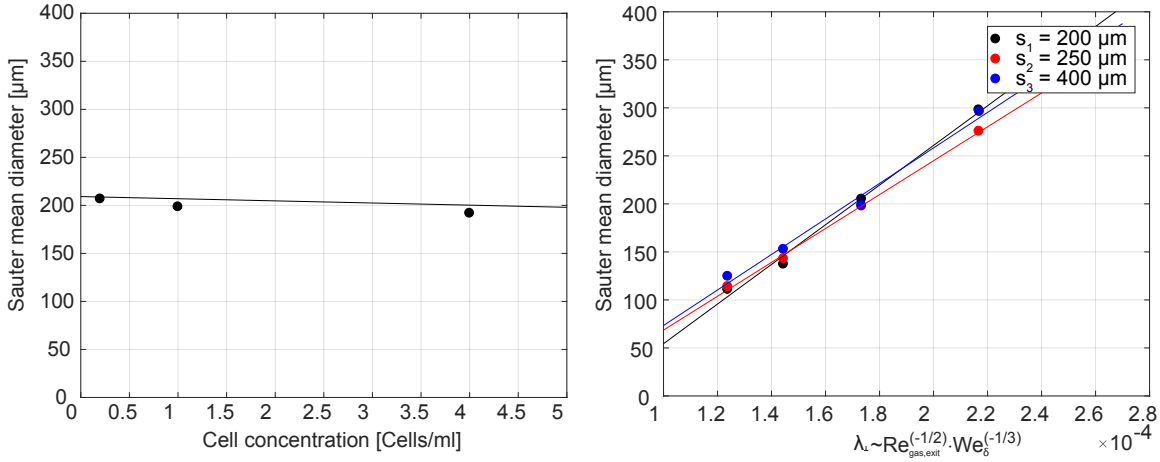

Figure 6. On the left Sauter mean diameter is presented over the cell concentration at operating point no. 1 and pipe no. 1. On the right, Sauter mean diameter is plotted over the transverse instability wavelength $\lambda_\perp$, which was derived by [16].

newtonian behavior. Thus, each following experiment is conducted using a cell concentration of 1×10^6 cells /mL, which on the one hand ensures a sufficient amount of cells for the determination of cell survival rates and on the other hand prevents consumptive usage of cells.

Table 3. Sauter mean diameter (SMD) and arithmetic mean diameter is given for s_1 = 400 µm in dependency of Re_{gas} and We

Reynolds number	Weber number	SMD [µm]	Arithmetic mean diameter [µm]
5529	4.41	297.9	102.3
6912	6.17	205	76.3
8294	8.12	137.2	59.4
9677	10.23	110.9	52.6

As stated in table 3, droplet sizes of coaxial atomizers decrease exponentially with increasing Reynolds number. Furthermore, increasing airflow causes an increase of interface acceleration shown by a growing value of the Weber number.

On the right side of figure 6 the Sauter mean diameter is plotted in dependency of the transverse instability wavelength $\lambda_\perp$. The latter was developed from Rayleigh-Taylor instabilites and is in dependency of Re and We. A detailed derivation of $\lambda_\perp$ can be seen in [16]. In short, $\lambda_\perp$ is a theoretical wavelength across the azimuthal angle of the spray cone and is calculated in dependency of the Reynolds and Weber number. Thereby, the Weber number has to be derived as function of the vorticity thickness δ (cf. equation 3). Droplet sizes represented by SMD increase linearly in proportion to $\lambda_\perp$, showing good agreement with earlier studies [9].

$$\delta \simeq 5.6 \cdot \Delta d \cdot \mathrm{Re}_{\mathrm{gas,exit}}^{-\frac{1}{2}} \qquad \text{leading to} \qquad \lambda_\perp \sim \mathrm{Re}_{\mathrm{gas,exit}}^{-\frac{1}{2}} \cdot \mathrm{We}_\delta^{-\frac{1}{3}} \tag{3}$$

In contrast, no noticeable impact of increasing wall thickness of the pipe on droplet sizes can be found. A possible explanation for this unexpected phenomenon is, that the diameter of the liquid phase does not match the inner diameter of the pipe (cf. figure 7). Instead, the liquid phase shows diameters comparable to the outer diameter d_a of the pipe. Note, that this effect even occurs for the largest values of s. This phenomenon is amongst other effects caused by capillary action, forcing the cell suspension to flow in radial direction towards the annular gas flow. Comprising, the annular gas flow is in direct contact with the liquid phase regardlessly of the wall thickness. Thus, interaction of the liquid and gas phase is not influenced by the varied parameter. Consequently, the process of inducing instabilities $\lambda_\perp$ on the liquid surface and hence the growth of ligaments are comparable between all pipes deployed in this study. This functional chain eventually leads to comparable droplet sizes also stated by [16].

Note, that besides having a constant diameter and thus showing comparable surface instabilities, the liquid jet is most likely characterized by different velocity fields.

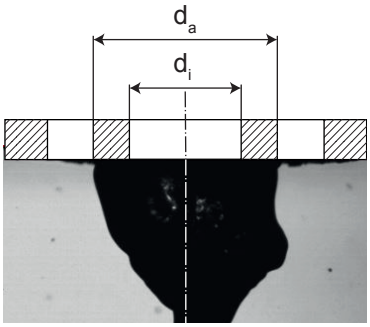

Figure 7. Microscopic view on the nozzle exit with d_i = 1.2 mm being the thinnest of the used pipes. The width of the liquid phase is noticeably larger than d_i reaching to the boundary with the annular gas flow.

Cell Survival Rates

The differences in cell survival rates across the radius of the spray cone are in the same order of magnitude as the indicated error bars. Thus, no dependency on the radius inside the spray cone can be found, as figure 8 states. Nevertheless, a certain influence of the radial position on cell survival rates cannot be fully suspended, since there is a big influence of mixing between the nozzle exit and the patternator located 100 mm beneath the nozzle exit. In order to determine this influence and to minimize the influence of mixing, the distance between patternator and nozzle exit has to be reduced to a minimum length in further studies.
Note, that the error bars for each point are derived as described in equation 4. Therefore, for each spray experiment taken, five measurements of cell survival rate are conducted in order to maximize the number of investigated cells.

$$ERR = \frac{1}{m}\sum_{i=1}^{m=5}\left|CSR_i - \overline{CSR}\right| \tag{4}$$

For each of these measurements, an individual value of CSR_i is taken, while $\overline{CSR}$ is derived by the ratio of all living cells counted with respect to all cells detected (cf. equation 5).

$$\overline{CSR} = \frac{\sum_{i=1}^{m=5} n_{\text{cells,living,i}}}{\sum_{i=1}^{m=5} n_{\text{cells,detected,i}}} \tag{5}$$

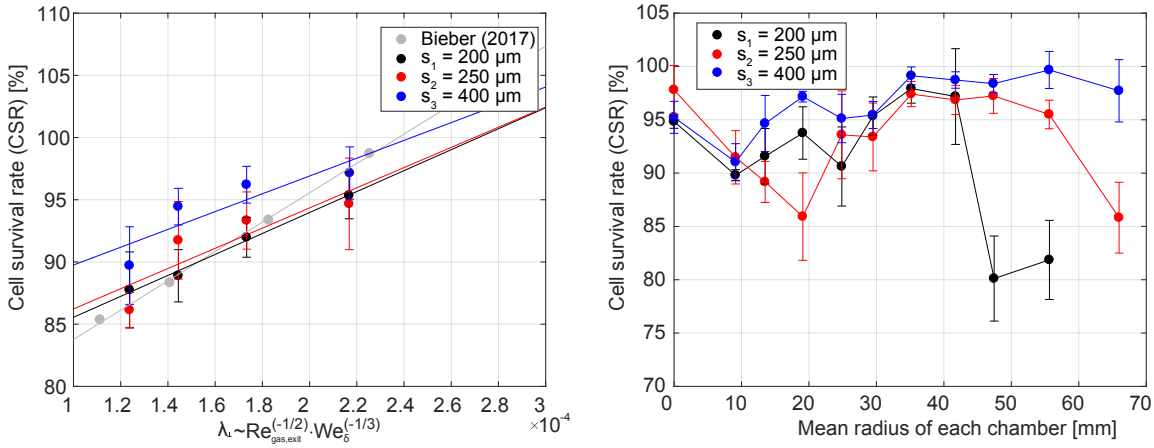

Figure 8. On the left, cell survival rates are presented in dependency of the transverse instability wavelength $\lambda_\perp$. The grey data points and line of best fit are taken from [9]. On the right, the cell survival rates for each wall thickness across the radius of the spray cone are given. Each point has been taken at $\dot{V}_{gas}$=1.5 $m^3\,h^{-1}$.

However, figure 8 also presents the cell survival rates in dependency of $\lambda_\perp$ considering data collected in this study and data generated in earlier studies. In both studies, the cell survival rates increase linearly in dependency of $\lambda_\perp$, showing different slopes. These differences are presumably caused by different cell types that were applied in both studies. While [9] used A549 cells with an average diameter of 15 µm, the SK-MEL-28 cells used in this study are distinctly bigger considering an average diameter of 19.4 µm. Furthermore, cell survival rates of the different pipes noticeably differentiate with increasing survival rates towards smaller inner diameters of the pipes und thus thicker walls seperating the liquid and gas flows. Note, the difference in CSR between pipe no. 1 and pipe no. 2 is noticeably smaller compared to pipe no. 1 and pipe no. 3, which can be explained by the difference in wall thickness ($\Delta s_{12} = 50\,\mu m$; $\Delta s_{13} = 200\,\mu m$). Since the diameter of the liquid phase stays constant for each pipe tested, a low velocity zone can be assumed beneath the walls as seen in figure 9. These low velocity zones increase in size with decreasing inner diameter leading to differences in local mass flow. Thus, for smaller values of d_i a smaller amount of cell suspension is directly exposed to surface instabilities close to the nozzle exit. Since the maximum of relative velocity between both phases is located at the nozzle exit, it is assumed that also the maxima of stresses and strains upon the liquid are located close to the nozzle exit. In contrast, the majority of droplets is formed further downstream (cf. red zone in figure 9). Since the variation of the nozzle has a minor impact on the droplet sizes for a given operating point, the differences of cell survival rates for different nozzles are most likely related to the formation of low velocity zones. However, droplet sizes are still of major interest for characterization of cell survival rates.

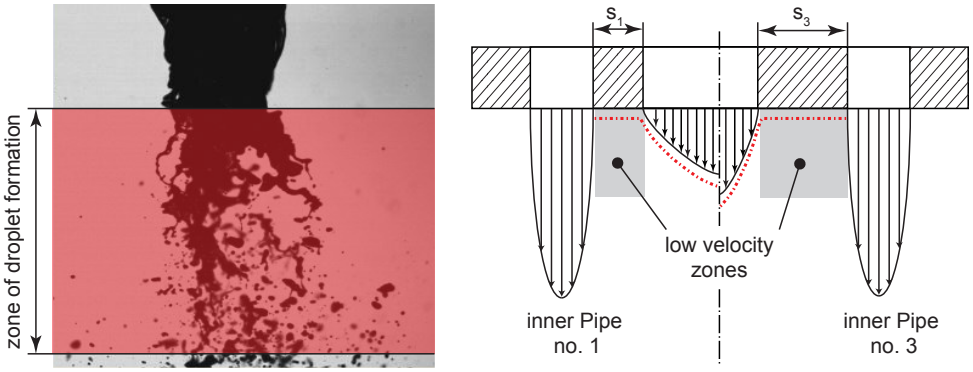

Figure 9. On the right, a schematic view is given also qualitatively showing velocities in the nozzle (black) and close to the exit (dotted, red) as well as locations of low velocity zones for different pipes.

Disintegration Lengths

On the left of figure 10 the disintegration length l_{dis} is presented in dependency of the d_i showing an increas of l_{dis} with increasing d_i. Furthermore, l_{dis} decreases with an increasing value of Re, which is caused by an increasing momentum flux of the gas phase.

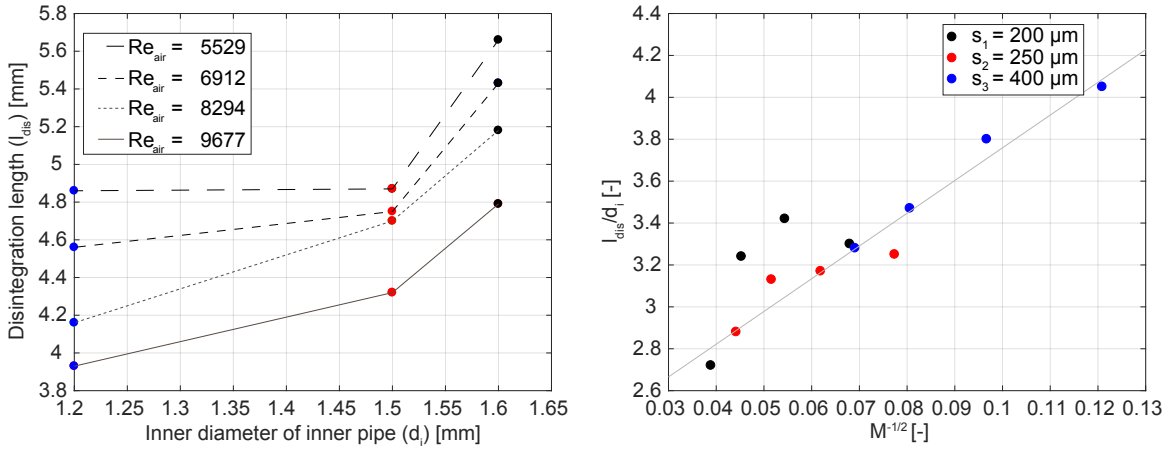

Figure 10. On the left, the disintegration length of the spray is given in dependency of the pipes inner diameter d_i for each Reynolds number set by the investigated test parameters. The right figure shows the ratio of disintegration length in respect to d_i in depency of $M^{-1/2}$. Note, that the line of best fit (grey) is presented for all measurements taken.

Lasheras et. al [19, 20] stated a correlation for the ratio between l_{dis} and d_i as shown in equation 6.

$$\frac{l_{\text{dis}}}{d_i} \propto \frac{1}{\sqrt{M}} \qquad \text{with M being calculated as} \qquad M = \frac{\rho_{\text{air}} \cdot u_{\text{air}}^2}{\rho_{\text{liq}} \cdot u_{\text{liq}}^2} \tag{6}$$

The right side of figure 10 shows the ratio between l_{dis} and d_i in dependency of $M^{-1/2}$ giving a linear proportionality. Hence, the increasing momentum flux of the liquid phase is responsible for an increasing ratio of l_{dis} to d_i and additionally to increasing cell survival rates. As mentioned above, this phenomenon is presumably caused by decreasing amounts of cells exposed to stresses caused by surface instabilities.
However, the actual disintegration length decreases for lower values of d_i (cf. figure 10). Overall, the breakup process can be divided into two regions. In vicinity to the nozzle, surface instabilities cause the formation of ligaments, which are then sheered of the liquid jet. At greater distances to the nozzle exit, small bulks of liquid are pinched of the liquid jet [20]. A decreasing value of d_i leads to a higher momentum and thus a smaller diameter at greater distances of the liquid jet. Lastly, a liquid jet with a smaller diameter is more likely to be pinched. This phenomenon leads to shorter disintegration lenths l_{dis} for smaller values of d_i.

Conclusions

The present work represents a systematic investigation of the impact of coaxial atomization with variation of nozzle design on characteristic parameters such as droplet sizes and disintegration lengths as well as cell survival rates. A whole range of experiments is conducted injecting cell suspensions containing living human cells with varying atomization conditions and nozzle designs. Additionally, experiments with different cell concentrations are conducted, ensuring the rheology of the injected liquid is not noticeably influenced by the investigated cell concentrations.

Droplet sizes are found not to be influenced by nozzle design, which leads to a general discussion of primary breakup phenomena regarding the liquid jet core diameter. The latter is determined to be constant for every nozzle design investigated, hence leading to the assumption of capillary action being responsible for the recorded effects. Cell survival rates are taken and discussed for each experiment in respect to nozzle design and radial position in the spray cone. Mixing effects occuring between nozzle exit and patternator are assumed to be responsible for a neglectable influence of radial position on cell survival rates. Further studies have to be conducted in order to fully determine the effect of the cells location in the liquid jet. Furthermore, the influence of wall thicknesses between both phases are found to be responsible for variations in the velocity fields in between both jets significantly affecting cell survival rates. The liquid bulk, which is directly interacting with the surrounding air flow, is characterized by low velocity zones which act protectively on the cells. With increasing values of the wall thickness, these low velocity zones grow in size leading to higher cell survival rates. This phenomenon corresponds well to the assumption, that cell survival rates are mainly affected by primary breakup and ligament formation, also supported by the proportional depency of cell survival rate on transverse instability wavelengths.
Lastly, disintegration lengths are discussed to be not affected by the phenomena mentioned above. Linear proportionality is found between the disintegration length and $M^{-1/2}$ being in good agreement with [19, 20]. In respect to the application of cell sprays in human airways, shortening the disintegration length is desirable to inhibit interactions between the liquid jet and walls of the airways.

Acknowledgements
This project was funded by the Deutsche Forschungsgemeinschaft (DFG, German Research Foundation) - Project no. RE 4092/2-1.

Nomenclature

T	Temperature [K]	s	Wall thickness [µm]	Re	Reynold number [–]
p	Pressure [N]	$\dot{V}$	Volume flow rate [$m^3\,h^{-1}$]	We	Weber number [–]
ρ	Density [$kg\,m^{-3}$]	$\dot{m}$	Mass flow rate [$kg\,s^{-1}$]	λ	Wavelength [m]
ν	Kinematic viscosity [$m^2\,s^{-1}$]	δ	Vorticity thickness [m]	CSR	Cell survival rate [%]
d, D	Diameter [mm]	u	Velocity [$m\,s^{-1}$]	M	Momentum flux ratio [–]

References

[1] Amini-Nik S., Dolp R., Eylert G., Datu A., Parousis A., Blakeley C., Jeschke M. G., 2018, *EBioMedicine*, 37, pp. 509-520.
[2] Ahmadi A. R., Chicco M. , Huang J., Qi L., Burdick J., Williams G. M., Cameron A. M., Sun Z., 2018, *Burns*.
[3] Kucharzewski M., Rojczyk E., Wilemska-Kucharzewska K., Wilk R., Hudecki J, Los M.J., 2019, *European Journal of Pharmacology*, 843, pp. 307-315.
[4] Quimby J. M., 2019, *Veterinary Clinics of North America: Small Animal Practice*, 49 (2), pp. 223-231.
[5] Thiebes, A. L., Albers, S., Klopsch, C., Jockenhoevel, S.,Cornelissen, C. G., 2015, *BioResearch open access*, 4(1), pp. 278–287.
[6] Gerlach, J. C., Johnen, C., McCoy, E., Bräutigam, K., Plettig, J., Corcos, A., 2011, *Burns*, 37(4), pp. e19–e23.
[7] Esteban-VivesR. , Corcos A., Choi M. S., Young M. T., Over P., Ziembicki J., Gerlach J. C., 2018, *Burns*, 44 (3). pp. 549-559.
[8] Thiebes, A. L., Reddemann, M. A., Palmer, J., Kneer, R., Jockenhoevel, S., Cornelissen, C. G., 2016, *Tissue Engineering Part C*, 22(4), pp. 322–331.
[9] Bieber M., Menzel S., Thiebes, A. L., Cornelissen, C. G., Jockenhoevel, S., Kneer R., Reddemann M. A., Sep. 6.-8. 2017, 28th Conference on Liquid Atomization and Spray Systems.
[10] Aguado, B., Mulyasasmita, W., Su, J., Lampe, K., Heilshorn, S., 2012, *Tissue Engineering Part A*, 18(7-8), pp. 806–815.
[11] Kuksin D., Chan L.,http://www.nexcelom.com/Applications/Cancer-Cells.html ([cit. 2013-12-06]).
[12] Tedeschi P., Markert E. Gounder M., et al, 2013, *Cell Death & Disease*, 4(877).
[13] Dolfi S., Chan L. Qiu J., et al., 2013, *Cancer & Metabolism*, 1(1).
[14] Ge, J., Guo, L., Wang, S., Zhang, Y., Cai, T., Zhao, R. C., Wu, Y., 2014, *Stem Cell Reviews and Reports*, 10(2), pp. 295-303.
[15] Bieber, M., Thiebes, L.,Cornelissen, C.G., Jockenhoevel, S., Kneer, R., Reddemann, M.A., Sep. 5.-7. 2016, 27th European Conference on Liquid Atomization and Spray Systems, Brighton, UK.
[16] Marmottant P., Villermaux E., 2004, *Journal of fluid mechanics*, 498, pp. 73–111.
[17] Bieber, M., Thiebes, L.,Cornelissen, C.G., Jockenhoevel, S., Kneer, R., Reddemann, M.A., 2017, *Atomization and Sprays, submitted*, 27 (10), pp. 847-858.
[18] Mayer W. O. H., 1994, *Experiments in Fluid*, 16, pp. 401-410.
[19] Lasheras J.C., Hopfinger E.J., 2000, *Annual Review of Fluid Mechanics*, 32, pp. 275-308.
[20] Lasheras J.C., Villermaux E., Hopfinger E.J., 1998, *Journal of Fluid Mechanics*, 357, pp. 351-379.